Robust Reactive Power Scheduling of Distribution Networks Based on Modified Bootstrap Technique

Liao, Wenlong; Wang, Shouxiang ; Bak-Jensen, Birgitte; Pillai, Jayakrishnan Radhakrishna; Yang, Zhe

Published in:
Journal of Modern Power Systems and Clean Energy

DOI (link to publication from Publisher):
10.35833/MPCE.2022.000850

Publication date:
2024

Document Version
Publisher's PDF, also known as Version of record

Robust Reactive Power Scheduling of Distribution Networks Based on Modified Bootstrap Technique

Wenlong Liao, Shouxiang Wang, Birgitte Bak-Jensen, Jayakrishnan Radhakrishna Pillai, and Zhe Yang

***Abstract*—The uncertainties of the power load, wind power, and photovoltaic power lead to errors between point prediction values and real values, which challenges the safe operation of distribution networks. In this paper, a robust reactive power scheduling (RRPS) model based on a modified bootstrap technique is proposed to consider the uncertainties of power loads and renewable energy sources. Firstly, a deterministic reactive power scheduling (DRPS) model and an RRPS model are formulated. Secondly, a modified bootstrap technique is proposed to estimate prediction errors of power loads and renewable energy sources without artificially assuming the probability density function of prediction errors. To represent all possible scenarios, point prediction values and prediction errors are combined to construct two worst-case scenarios in the RRPS model. Finally, the RRPS model is solved to find a scheduling scheme, which ensures the security of distribution networks for all possible scenarios in theory. Simulation results show that the worst-case scenarios constructed by the modified bootstrap technique outperform popular baselines. Besides, the RRPS model based on the modified bootstrap technique balances economics and security well.**

***Index Terms*—Distribution network, worst-case scenario, robust programming, prediction error, bootstrap technique.**

I. Introduction

REACTIVE power scheduling aims to reduce active power losses of distribution networks and maintain the desired voltage level by regulating different power devices such as transformers, distributed generators (DGs), and shunt capacitor banks. Reactive power scheduling is generally regarded as a special case of optimal power flow, which plays an important role in the safe and economic operation of distribution networks [1].

The traditional reactive power scheduling is formulated as a deterministic model, in which the input data (e.g., deterministic point prediction values of power loads and renewable energy sources) are assumed to be ideally accurate. Prediction errors (also called uncertainty sets in some publications) are ignored. Practically, the prediction errors of power loads are unavoidable due to various reasons such as insufficient real-time measurements in distribution networks, state estimations heavily dependent on pseudo measurements, and changing consumption habits [2]. In addition, real output power of renewable energy sources varies with meteorological factors (e.g., wind speed, wind direction, and light intensity), which fluctuates frequently. In such situations, the traditional deterministic reactive power scheduling (DRPS) model has difficulty in ensuring the security of distribution networks [3], especially when prediction errors of power loads and renewable energy sources are large.

To account for the prediction errors of power loads and renewable energy sources, fuzzy optimization, stochastic optimization, interval optimization, and robust optimization have been extensively explored. For example, a fuzzy logic control model and a particle swarm optimization method are combined to minimize tie-line power flow in [4]. The work in [5] employs the Weibull distribution to represent wind power uncertainty by producing a set of scenarios. To consider the fluctuation of loads in one day, a new interval power flow analysis is proposed to obtain the accurate ranges of interval state variables in [6]. Generally, the solutions of fuzzy optimization, stochastic optimization, and interval optimization are not always feasible for all possible combinations of load conditions and output power of renewable energy sources. In contrast, robust optimization attempts to find such guaranteed feasible solutions by constructing worst-case scenarios. The worst-case scenarios are utilized to obtain an optimal solution. If the solution can ensure the security of distribution networks in worst-case scenarios, it should also be applicable to other possible scenarios [7]. In view of this, there are an increasing number of robust optimization applications in distribution networks.

The main challenge in robust reactive power scheduling (RRPS) of distribution networks is to construct worst-case scenarios. Traditionally, the worst-case scenarios are divided into two categories [8]: ① the maximum power loads and the minimum output power of renewable energy sources; and ② the minimum power loads and the maximum output power of renewable energy sources. Obviously, this traditional method is too simple, and even it does not use any point prediction value when constructing these two categories of worst-case scenarios. The reactive power scheduling scheme

Manuscript received: December 27, 2022; revised: February 20, 2023; accepted: April 6, 2023. Date of CrossCheck: April 6, 2023. Date of online publication: May 19, 2023.

W. Liao, B. Bak-Jensen, J. R. Pillai, and Z. Yang (corresponding author) are with the AAU Energy, Aalborg University, Aalborg 9220, Denmark (e-mail: weli@energy.aau.dk; bbj@energy.aau.dk; jrp@energy.aau.dk; zya@energy.aau.dk).

S. Wang is with the Key Laboratory of Smart Grid, Ministry of Education, School of Electrical and Information Engineering, Tianjin University, Tianjin 300072, China (e-mail: sxwang@tju.edu.cn).

DOI: 10.35833/MPCE.2022.000850

based on this traditional method is too conservative, that is, it loses the economy of distribution networks.

To balance economy and security, a large number of publications have focused on constructing the worst-case scenarios in recent years. Normally, the worst-case scenario construction consists of point prediction and prediction error estimation. The worst-case scenarios are constructed by adding point prediction values and prediction errors. This paper focuses on the latter one (i.e., the prediction error estimation).

To represent the prediction errors of power loads and wind power, a Gaussian distribution model is proposed in [9]. The prediction errors of wind power are assumed to obey the Laplace distribution in [10], and the Latin hypercube sampling algorithm is utilized to produce possible scenarios. To describe the variation of wind speed, the Rayleigh distribution and Weibull distribution are integrated in [11] and [12]. Similarly, the Beta distribution is employed to capture the uncertainty of the photovoltaic (PV) output power, and then the Monte Carlo method is used to sample possible errors in [13]. Other popular distributions such as the Cauchy distribution are presented in [14], and the mixed Laplace distribution is adopted in [15]. However, the prediction errors of power loads and renewable energy sources vary from meteorological factors, point prediction models, and geographical locations, leading to no uniform and accurate probability density function (PDF) exists to describe the real distribution in different scenarios.

Generally, these existing methods cannot accurately estimate prediction errors. If the estimated prediction errors are much greater than real errors, the worst-case scenarios will be too conservative (i.e., the solution loses economy). Conversely, if the estimated prediction errors are much smaller than real values, the worst-case scenarios cannot represent all possible scenarios (i.e., the solution loses security). It remains a challenge to accurately estimate prediction errors without assuming and sampling PDFs for the RRPS model of distribution networks.

Bootstrap technique is a popular method, which is widely used to estimate uncertainty (confidence interval, prediction error, variance, bias, etc.) by random sampling with replacement [16]. One of the advantages of the bootstrap technique over traditional methods is that it does not require artificial assumptions about the empirical PDF [17]. As long as the sampled errors and the real errors obey the same distribution, the bootstrap technique can accurately represent the uncertainty of the observed data. These advantages make the bootstrap technique a perfect candidate to estimate the prediction errors for the RRPS model of distribution networks. However, there are two limitations of the traditional bootstrap technique that need to be addressed.

Firstly, the prediction errors estimated by the traditional bootstrap technique are often smaller than the real prediction errors. Secondly, the traditional bootstrap technique requires a sufficiently large sample size for the new error set, which imposes a tedious sampling process.

To fill the knowledge gap, this paper proposes a new kind of RRPS model of distribution networks based on the modified bootstrap technique. The key contributions are summarized as follows.

1) Accuracy prediction errors are estimated by a new kind of bootstrap technique, which does not require artificial assumptions about the PDF. To accommodate prediction error estimation for the RRPS model, some necessary modifications are made to address the two gaps in the traditional bootstrap technique.

2) After estimating prediction errors, two worst-case scenarios are constructed to represent all possible scenarios in the RRPS model.

3) An RRPS model is formulated to fully account for the uncertainties of power loads and renewable energy sources by considering operational constraints in worst-case scenarios.

The rest of this paper is organized as follows. Section II formulates the DRPS model. Section III introduces the RRPS model. Simulations are performed to test the performance of the proposed RRPS model based on the modified bootstrap technique in Section IV. Finally, Section V summarizes conclusions and presents future works.

II. DRPS Model

The reactive power scheduling of distribution networks generally aims to reduce active power losses and maintain the voltage profiles in a safe range by controlling transformer taps and reactive power compensators within a given time frame [18], [19].

Normally, the reactive power compensators can be categorized into discrete control devices, e. g., shunt capacitor banks (CBs) and continuous control devices (e.g., DGs). The states of shunt CBs and transformer taps cannot be regulated frequently owing to the limitations of existing manufacturing technologies and the lifetime of control devices. Similar to the previous study [20], the maximum allowable action times of control devices are considered by adding action costs into the objective function. Specifically, the DRPS model is defined as follows [21].

1) Objective function

$$\min F = C_{\text{loss}} \sum_{t=1}^{24} P_{\text{loss},t} \Delta t + C_{\text{CB}} \sum_{i=1}^{n_{\text{C}}} \sum_{t=2}^{24} \left(Q_{\text{CB},i,t-1} \oplus Q_{\text{CB},i,t} \right) + C_{\text{T}} \sum_{i=1}^{n_{\text{T}}} \sum_{t=2}^{24} \left(T_{i,t-1} \oplus T_{i,t} \right) \tag{1}$$

$$P_{\text{loss},t} = \sum_{i=1}^{n} G_{ij} \left(U_{i,t}^2 + U_{j,t}^2 - 2U_{i,t}U_{j,t} \cos\left(\theta_{i,t} - \theta_{j,t} \right) \right) \tag{2}$$

where F is the objective function, including the operational cost of power losses, the action cost of shunt CBs, and the action cost of transformer taps; C_{loss} is the price of energy loss; C_{CB} is the price of a single adjustment of CBs; C_{T} is the price of a single adjustment of the transformer tap; n_{T} is the number of transformers in distribution networks; n_{C} is the number of shunt CBs in distribution networks; $Q_{\text{CB},i,t}$ is the reactive power output provided by shunt CB i at time t; $T_{i,t}$ is the tap ratio of transformer i at time t; $\oplus$ is the exclusive operation, whose value is 1 only if its arguments differ; Δt is the time horizon, which is usually 1 hour; $P_{\text{loss},t}$ is the active power loss at time t; n is the number of distribution lines; $\theta_{i,t}$ is the voltage phase angle of bus i at time t; $U_{i,t}$ is the voltage magnitude of bus i at time t; and G_{ij} is the mutu-

al conductance of distribution line from bus i to bus j.

2) Power flow constraints

$$\begin{cases} P_{i,t}-P_{\mathrm{DG},i,t}-U_{i,t}\sum_{j=1}^{m}U_{j,t}\left(G_{ij}\cos\theta_{ij,t}+B_{ij}\sin\theta_{ij,t}\right)=0 \\ Q_{i,t}-Q_{\mathrm{CB},i,t}-Q_{\mathrm{DG},i,t}-U_{i,t}\sum_{j=1}^{m}U_{j,t}\left(G_{ij}\sin\theta_{ij,t}-B_{ij}\cos\theta_{ij,t}\right)=0 \end{cases} \tag{3}$$

where $P_{i,t}$ and $Q_{i,t}$ are the active and reactive power loads of bus i at time t, respectively; $P_{\mathrm{DG},i,t}$ and $Q_{\mathrm{DG},i,t}$ are the active and reactive power outputs provided by DGs of bus i at time t, respectively; B_{ij} is the mutual susceptance of distribution line from bus i to bus j; $\theta_{ij,t}$ is the voltage phase angle of distribution line from bus i to bus j at time t; and m is the number of buses.

3) Current constraints

$$I_{i,t}\le I_{\max,t}\quad i=1,2,\ldots,n \tag{4}$$

where $I_{\max,t}$ is the maximum allowable current of distribution line i; and $I_{i,t}$ is the current of distribution line i at time t.

4) Voltage constraints

$$U_{\min,i}\le U_{i,t}\le U_{\max,i}\quad i=1,2,\ldots,m \tag{5}$$

where $U_{\min,i}$ and $U_{\max,i}$ are the minimum and maximum allowable voltages of bus i, respectively.

5) Transformer constraints

$$T_{\min,i}\le T_{i,t}\le T_{\max,i}\quad i=1,2,\ldots,n_{\mathrm{T}} \tag{6}$$

where $T_{\min,i}$ and $T_{\max,i}$ are the minimum and maximum tap ratios of transformer i, respectively.

6) DG constraints

$$Q_{\mathrm{DG},i,t}\le Q_{\mathrm{DG},i,t,\max}=\sqrt{S_{\mathrm{DG},i}^2-P_{\mathrm{DG},i,t}^2}\quad i=1,2,\ldots,n_{\mathrm{DG}} \tag{7}$$

where $Q_{\mathrm{DG},i,t,\max}$ is the maximum reactive power output provided by DG i at time t; n_{DG} is the number of DGs in distribution networks; and $S_{\mathrm{DG},i}$ is the maximum apparent power (i.e., capacity) of DG i.

The capability curve of a DG is depicted in Fig. 1 [22]. The maximum reactive power output $Q_{\mathrm{DG,max}}$ is limited by the capacity S_{DG} and active power output P_{DG} of the DG. Besides, the reactive power outputs provided by DGs can be leading or lagging power.

Note that (7) represents the DGs operating in the widely used P-Q control mode [23], while the DGs operating in other control modes (e.g., P-V control mode) can be easily added in future works.

7) CB constraints

$$0\le Q_{\mathrm{CB},i,t}\le Q_{\mathrm{CB},i,\max}\quad i=1,2,\ldots,n_{\mathrm{C}} \tag{8}$$

where $Q_{\mathrm{CB},i,\max}$ is the maximum reactive power output provided by the shunt CB i.

In summary, the framework of the proposed DRPS model is shown in Fig. 2. The objective function is to minimize the operational cost given the deterministic point prediction values of load conditions and renewable energy sources. The variables to be optimized include the transformer tap ratio, number of operational CBs, and reactive power output of DGs at each time horizon given a set of operational constraints. Note that more objective functions (e.g., voltage deviation) as well as control devices (e.g., heat pumps, energy storage, and electric vehicles) can be added to the above DRPS model in extended work [24].

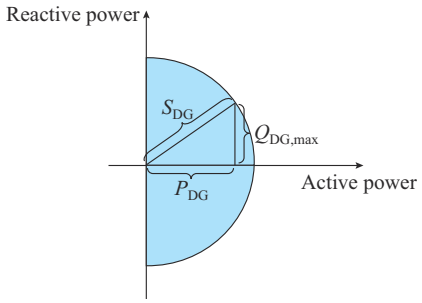

Fig. 1. Capability curve of a DG.

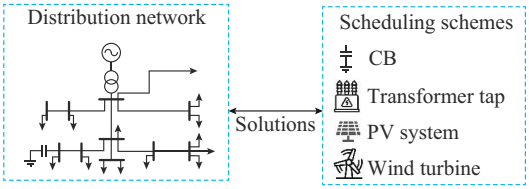

Fig. 2. Framework of proposed DRPS model.

III. RRPS Model

The focus of this paper is on the construction of the worst-case scenario for the RRPS model. First, a modified bootstrap technique is proposed to estimate prediction errors accurately. Then, the upper and lower boundaries of these prediction errors and the point prediction values are combined to form two worst-case scenarios, representing the full range of possible scenarios. Finally, the DRPS model is generalized to the RRPS model considering worst-case scenarios.

A. Prediction Error Estimation

The point prediction models only provide a single most likely value to estimate the power loads or output power of renewable energy sources, which brings risks to the safe operation of distribution networks due to ignoring the uncertainty.

As an advanced method of error estimation, the bootstrap technique employs upper and lower boundaries to represent the uncertainty of a single prediction value without assuming the PDF of prediction errors. In particular, Fig. 3 presents the framework of the standard bootstrap technique. The prediction error estimation of the point prediction values by using the standard bootstrap technique consists of three main steps [16].

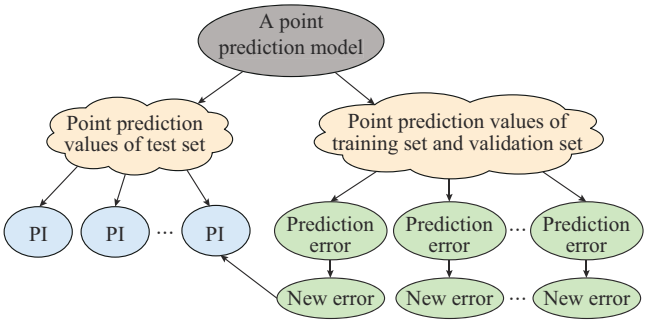

Fig. 3. Framework of standard bootstrap technique.

1) Calculate prediction errors of the training set and validation set. First, a point prediction model is trained to obtain point prediction values of the training set, validation set, and test set. Then, the prediction errors of the training set and validation set can be obtained by calculating the Euclidean distance between the real values and point prediction values. The prediction errors of the training set and validation set are used to construct the prediction intervals (PIs) of the test set.

2) Construct an error set. To obtain the PIs of the test set, prediction errors of the training set and validation set are sampled (sampled with replacement) to obtain a new error set. The number of samples in the new error set should be large enough to ensure statistical significance (the more samples the better, if there are enough computing resources), generally tens of thousands of times.

3) Construct PIs for the test set. The new error set is sorted in descending order, and then the lower and upper boundaries are determined by selecting a value at the percentile α for the confidence level (CL). For example, if the CL is set to be 95%, the percentile α would be 0.95. The value at the 2.5% percentile of this new error set is considered as the lower boundary, and the value at the 97.5% percentile of this new error set is regarded as the upper boundary.

To accommodate the prediction error estimation of the RRPS model, the standard bootstrap technique in this paper is modified in the following two aspects, and the framework of the modified bootstrap technique is shown in Fig. 4.

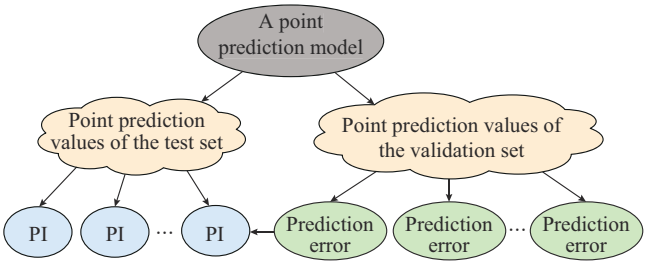

Fig. 4. Framework of modified bootstrap technique.

1) The prediction error of the training set is removed. The reason is that the training set has been used to train the point prediction model, which results in smaller prediction errors in the training set than those in the test set. In particular, the difference in prediction errors can be large between the training set and test set, if the point prediction model suffers from severe over-fitting problems.

2) The second step of the standard bootstrap technique requires a sufficiently large sample size for the new error set, which imposes a tedious sampling process. Fortunately, if the number of samples is infinite, the new error set will have the same probability distribution as the prediction errors in the validation set (i.e., the quantile of the new error set is the same as the prediction error set in the validation set). In other words, the new error set is redundant, and it can be replaced by the prediction errors in the validation set ignoring the second step of the standard bootstrap technique. Therefore, the prediction error set in the validation set can be sorted in descending order to construct the PIs of the test set, and then the lower and upper boundaries are determined by selecting a value at the percentile α for the CL.

Note that both traditional and modified bootstrap techniques share the same hypothesis that the data distributions in the training, validation, and test sets are similar [25]. Only in this case, the prediction errors of the validation and test sets can be small, and the prediction errors of the test set can be accurately estimated by those of the validation set. Besides, the data size of the training set should be large enough (e.g., several thousands of samples) to train a good point prediction model, and the data size of the validation set should also be large enough to accurately estimate the prediction errors of the test set.

B. Worst-case Scenario Construction

So far, prediction errors of point prediction values can be represented as PIs by the modified bootstrap technique described above. The next important aspect is to construct the worst-case scenarios for the RRPS model of distribution networks. If the scheduling scheme is suitable for the worst-case scenarios (also called extreme scenarios in some studies), it also should be suitable for other possible scenarios. Therefore, the worst-case scenarios are generally used to represent all possible scenarios in the RRPS model. Normally, the worst-case scenarios include the following two cases [9].

Case 1: the real power loads are larger than the point prediction values, while the real output power of the renewable energy sources is smaller than the point prediction values.

Specifically, the power load can be represented as a sum of point prediction values and upper boundaries of prediction errors, as shown in the upper boundary of the blue area in Fig. 5. The output power of renewable energy sources can be represented as a sum of point prediction values and lower boundaries of prediction errors, as shown in the lower boundary of the blue area in Fig. 6. This case can be formulated as:

$$\begin{cases} P_{\text{Case1},i,t} = P_{i,t} + \Delta P_{\text{Up},i,t} & i = 1,2,\ldots,m \\ Q_{\text{Case1},i,t} = Q_{i,t} + \Delta Q_{\text{Up},i,t} & i = 1,2,\ldots,m \end{cases} \tag{9}$$

$$P_{\text{Case1,DG},i,t} = P_{\text{DG},i,t} + \Delta P_{\text{Low,DG},i,t} \quad i = 1,2,\ldots,m \tag{10}$$

where $P_{\text{Case1},i,t}$ and $Q_{\text{Case1},i,t}$ are the active and reactive power loads of bus i at time t for case 1, respectively; $\Delta P_{\text{Up},i,t}$ and $\Delta Q_{\text{Up},i,t}$ are the upper boundaries of prediction errors for active and reactive power loads of bus i at time t, respectively; $P_{\text{Case1,DG},i,t}$ is the active power output provided by DG i at time t for case 1; and $\Delta P_{\text{Low,DG},i,t}$ is the lower boundary of the prediction error of the active power output provided by DG i at time t.

Case 2: the active power loads are smaller than the point prediction values, while the active power output of the renewable energy sources is larger than the point prediction values.

Specifically, the power load can be represented as a sum of point prediction values and low boundaries of prediction errors, as shown in the lower boundary of the blue area in Fig. 5. The power output of renewable energy sources can be represented as a sum of point prediction values and upper boundaries of prediction errors, as shown in the upper

boundary of the blue area in Fig. 6. This case can be formulated as:

$$\begin{cases} P_{\text{Case 2},i,t} = P_{i,t} + \Delta P_{\text{Low},i,t} & i = 1,2,\ldots,m \\ Q_{\text{Case 2},i,t} = Q_{i,t} + \Delta Q_{\text{Low},i,t} & i = 1,2,\ldots,m \end{cases} \tag{11}$$

$$P_{\text{Case 2,DG},i,t} = P_{\text{DG},i,t} + \Delta P_{\text{Up,DG},i,t} \quad i = 1,2,\ldots,m \tag{12}$$

where $P_{\text{Case2},i,t}$ and $Q_{\text{Case2},i,t}$ are the active and reactive power loads of bus i at time t for case 2, respectively; $\Delta P_{\text{Low},i,t}$ and $\Delta Q_{\text{Low},i,t}$ are the lower boundaries of prediction errors for active and reactive power loads of bus i at time t, respectively; $P_{\text{Case2,DG},i,t}$ is the active power output provided by DG i at time t for case 2; and $\Delta P_{\text{Up,DG},i,t}$ is the upper boundary of prediction errors of the active power output provided by DG i at time t.

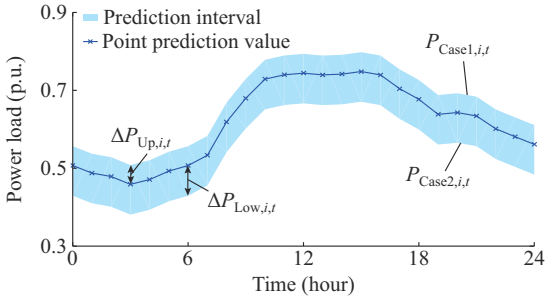

Fig. 5. Visualization of active power loads.

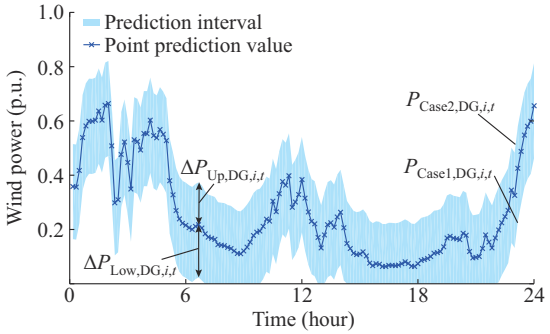

Fig. 6. Visualization of wind power.

In summary, two worst-case scenarios have been constructed based on the modified bootstrap technique. Unlike previous studies [9]-[12], the modified bootstrap technique does not need to assume the PDF of prediction errors.

C. RRPS Model

After constructing two worst-case scenarios, the RRPS model is formulated to search for solutions, which should ensure the security of distribution networks in point prediction values and two worst-case scenarios. The framework of the RRPS model is shown in Fig. 7.

Specifically, the point prediction value scenarios are most likely to occur, while the worst-case scenarios are rare. Therefore, the objective function of the RRPS model is defined to be consistent with the DRPS model, i.e., (1).

Furthermore, the constraints of the RRPS model include not only the constraints (3)-(8) of the DRPS model, but also the constraints in two worst-case scenarios:

$$I_{\text{Case 1},i,t} \le I_{\max,t} \quad i = 1,2,\ldots,n \tag{13}$$

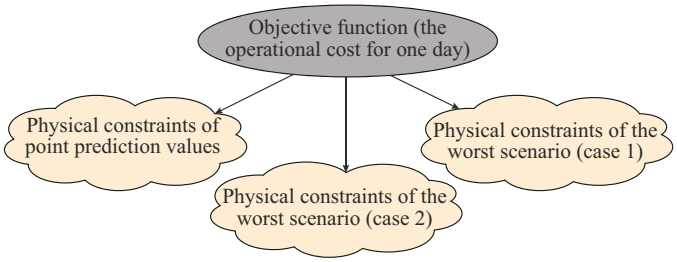

Fig. 7. Framework of RRPS model.

$$I_{\text{Case 2},i,t} \le I_{\max,t} \quad i = 1,2,\ldots,n \tag{14}$$

$$U_{\min,i} \le U_{\text{Case 1},i,t} \le U_{\max,i} \quad i = 1,2,\ldots,m \tag{15}$$

$$U_{\min,i} \le U_{\text{Case 2},i,t} \le U_{\max,i} \quad i = 1,2,\ldots,m \tag{16}$$

$$Q_{\text{DG},i,t} \le Q_{\text{DG},i,t,\max} = \sqrt{S_{\text{DG},i}^2 - P_{\text{Up,DG},i,t}^2} \quad i = 1,2,\ldots,n_{\text{D}} \tag{17}$$

where $I_{\text{Case1},i,t}$ and $I_{\text{Case2},i,t}$ are the currents of distribution line i at time t for cases 1 and 2, respectively; and $U_{\text{Case1},i,t}$ and $U_{\text{Case2},i,t}$ are the voltage magnitudes of bus i at time t for cases 1 and 2, respectively.

Note that the constraints (13)-(16) ensure that the solution is also feasible for two worst-case scenarios, and the constraint (17) describes the maximum reactive power output of DGs, which is limited by the active power output of DGs.

Up to this point, the RRPS model has been formulated. By solving this model, the obtained solution ensures the security of distribution networks for all possible scenarios in theory.

IV. Case Study

A. Simulation Details

To verify the effectiveness of the proposed modified bootstrap technique for the RRPS model of distribution networks, simulations and analyses are performed on an IEEE 33-bus distribution network, whose parameters can be founded in [26]. Further, various control devices such as the CB, transformer, PV system, and wind turbine (WT) are added to the feeders, as shown in Fig. 8.

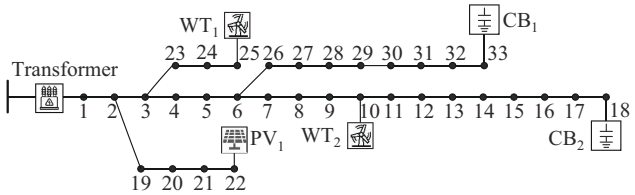

Fig. 8. Framework of IEEE 33-bus distribution network.

In particular, the voltage base value is 12.66 kV. The transformer tap includes 9 ratios, which vary from $-4 \times 1.25\%$ to $4 \times 1.25\%$. Various control devices are generally decentralized and located at the end of feeders to reduce power loss and boost voltage. Therefore, this paper makes the following assumptions about the location and capacity of DGs and CBs: WTs are added to the 10th bus and 25th bus. A PV system is added to the 22nd bus. The maximum apparent power (i.e., capacity) of the PV system and WTs is 300 kVA. The

reactive power outputs provided by DGs (i. e., PV system and WTs) can be leading or lagging power. Both the 18th bus and the 33rd bus are added with 5 CBs (denoted as CB_1 and CB_2). The reactive power provided by each CB is 100 kvar. The safe voltages at all buses range from 0.95 p.u. to 1.05 p.u.. The electricity price is 0.5 ¥/kWh, and the price of a single adjustment of the CBs and the transformer tap is ¥6 [20]. The maximum allowable action times over 24 hours are 5 and 4 for CBs and transformer taps, respectively [27].

The original IEEE 33-bus distribution network only includes one moment of loads, which cannot be used to train the point prediction model. The London smart meter dataset is employed to construct the power load for each bus [28]. Specifically, this dataset includes hourly load curves of 112 blocks. To simulate the nodal loads of the distribution network, loads of three neighboring blocks are combined and then scaled appropriately as the load data of a bus in the distribution network. The 1st bus is the slack bus. The data from the first 96 blocks are used to simulate the power loads from the 2nd bus to 33rd bus. Since there are different time ranges of power loads in different blocks, the power loads from January to June 2012 are used for simulation and analysis. Hourly PV generation curves and hourly wind generation curves are selected from the National Renewable Energy Laboratory [29], [30]. For power loads and renewable energy sources, the first 80% of the data in each month constitutes the training set, and the last 10% of the data in each month constitutes the test set. The middle 10% of the data in each month constitutes the validation set.

Point prediction, prediction error estimation, and worst-case scenario construction are implemented in the Python, including Spektral 1.0 and Tensorflow 2.0. The power flow analysis is performed in MATLAB 2018a using a computer with the CPU of Intel Core i5-8265U (base frequency is 1.80 GHz) and the RAM of 8 GB.

The DRPS model and RRPS model are solved by a genetic algorithm. Specifically, to ensure the operational constraints, the penalty method is employed to transform constrained models into an unconstrained model. In addition, the coding method (i.e., how to initialize the chromosome in the genetic algorithm) of various power devices can be found in [31].

B. Feasibility Analysis of Prediction Error Estimation

The prediction error estimation directly affects the quality of the worst-case scenarios. Only when the constructed PIs cover enough real values can the worst-case scenarios represent all possible scenarios. In this subsection, the effectiveness of the proposed modified bootstrap technique for prediction error estimation is demonstrated.

Specifically, the time-series predictions of power loads in the 2nd bus, wind power in the 10th bus, and PV power in the 22nd bus are considered as simple examples. First, a point prediction model named gated recurrent unit is employed to predict power loads, wind power, and PV power, because of its outstanding ability in time-series prediction [25], [32]. Then, the PDFs of prediction errors of the training, validation, and test sets using the power load, wind power, and PV power datasets are visualized, as shown in Figs. 9-11.

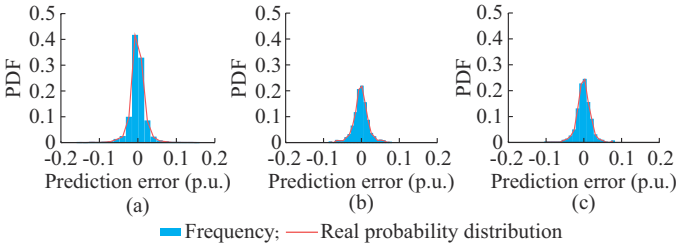

Fig. 9. PDFs of prediction errors of training, validation, and test sets using power load dataset. (a) Training set. (b) Validation set. (c) Test set.

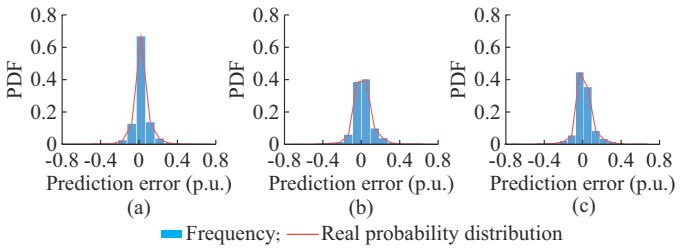

Fig. 10. PDFs of prediction errors of training, validation, and test sets using wind power dataset. (a) Training set. (b) Validation set. (c) Test set.

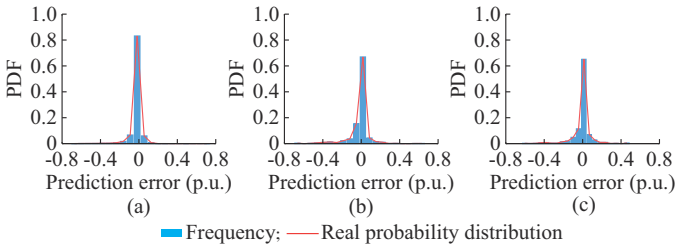

Fig. 11. PDFs of prediction errors of training, validation, and test sets using PV power dataset. (a) Training set. (b) Validation set. (c) Test set.

Comparing Fig. 9(a) and Fig. 9(c), it is clear that the average prediction error of the training set is smaller than that of the validation and test sets. The reason is that the samples in the training set have been used to train the point prediction model, and any point prediction model involves over-fitting problems to some extent. Normally, the better the generalization of a point prediction model, the closer the prediction error between the training and test sets.

Further, if the prediction error of the training set is used to estimate prediction errors of the test set, the obtained PIs will be too narrow to cover possible scenarios, and the security of distribution networks cannot be ensured. This shows that the modifications (i.e., prediction errors of the training set are not used to estimate prediction errors of the test set) to the traditional bootstrap technique in this paper are necessary.

Relatively, the prediction errors of the validation set and test set are very similar, which can be verified by comparing Fig. 9(b) and Fig. 9(c). This is because both the validation and test sets are not used to train the point prediction model, and they have similar data distributions. Further, the prediction errors of the validation set and test set obey the same distribution, which is why the modified bootstrap technique only uses the prediction errors of the validation set to estimate those of the test set.

Note that the above analysis and conclusions on power loads are also applicable to wind power and PV power, which can be verified by observing Fig. 10 and Fig. 11.

To demonstrate the performance of the proposed modified bootstrap technique, the widely used ensemble Gaussian model in [33] and the traditional bootstrap technique are considered as baselines. First, the prediction errors of power loads, wind power, and PV power are estimated based on the bootstrap techniques and the ensemble Gaussian model at different CLs. PIs of power loads and renewable energy sources are obtained by combining point prediction values and prediction errors. Then, the popular indicators such as prediction interval coverage percentage (PICP) and prediction interval normalized average width (PINAW) in [2] are selected to evaluate PIs. The PICP describes the probability that PIs cover the real value, while PINAW represents the width of PIs. The larger the PICP, the better the uncertainty set. The smaller the PINAW, the better the uncertainty set. Finally, indicators of PIs generated by different models are calculated, as shown in Table I.

Besides, an hourly power load curve, an hourly wind power generation curve, and an hourly PV power generation curve are randomly selected for visualization, as shown in Figs. 12-14.

TABLE I
INDICATORS OF PIS GENERATED BY DIFFERENT MODELS

Dataset	CL (%)	Modified bootstrap technique		Traditional bootstrap technique		Ensemble Gaussian model	
		PICP (%)	PINAW (p.u.)	PICP (%)	PINAW (p.u.)	PICP (%)	PINAW (p.u.)
Power load	60	61.53	0.023	57.88	0.021	48.12	0.018
	80	84.12	0.041	75.41	0.034	64.71	0.026
	90	91.18	0.060	86.94	0.053	74.76	0.034
	99	99.53	0.136	97.94	0.133	88.24	0.059
Wind power	60	63.25	0.087	57.67	0.070	28.42	0.046
	80	83.58	0.169	77.58	0.139	40.33	0.088
	90	91.08	0.251	87.83	0.218	50.92	0.101
	99	98.83	0.572	98.92	0.566	68.33	0.156
PV power	60	64.00	0.011	58.82	0.008	66.82	0.028
	80	83.76	0.050	79.88	0.046	76.12	0.042
	90	92.47	0.118	87.41	0.113	82.65	0.049
	99	99.06	0.239	97.41	0.186	95.88	0.125

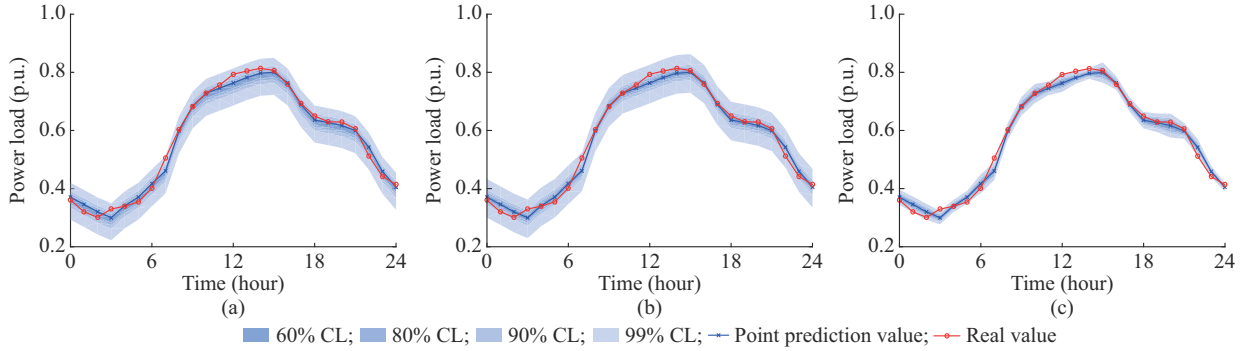

Fig. 12. Prediction errors and real values of power loads at different CLs when using modified bootstrap technique, traditional bootstrap technique, and ensemble Gaussian model. (a) Modified bootstrap technique. (b) Traditional bootstrap technique. (c) Ensemble Gaussian model.

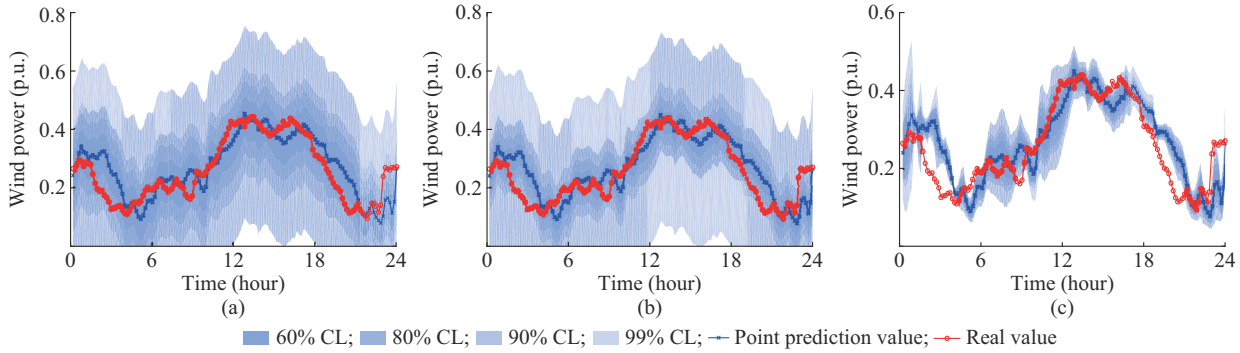

Fig. 13. Prediction errors and real values of wind power at different CLs when using modified bootstrap technique, traditional bootstrap technique, and ensemble Gaussian model. (a) Modified bootstrap technique. (b) Traditional bootstrap technique. (c) Ensemble Gaussian model.

1) Comparison analysis between modified bootstrap technique and ensemble Gaussian model

It is obvious that the PIs (i.e., the combination of point prediction values and prediction errors) generated by the ensemble Gaussian model have difficulty in covering the real scenarios, since its PICP is much smaller than the CL (i.e., the expected probability covers the real values). Although the PINAW of the modified bootstrap technique is larger than that of the ensemble Gaussian model at the same CL, the PICP of the modified bootstrap technique is close to the CL and much larger than that of the ensemble Gaussian model. This indicates that the modified bootstrap technique can accurately capture the uncertainties in power loads, wind power, and PV power. For example, for the prediction errors of power loads with 99% CL, the PICP of the ensemble Gaussian model is 88.24%, while that of the modified boot-

strap technique is 99.53%. If the prediction errors estimated by the ensemble Gaussian model are used for the RRPS model, the solution is difficult to ensure the security of the distribution network. In contrast, the RRPS solution based on the prediction errors generated by the modified bootstrap technique has a higher probability to ensure the security of the distribution network.

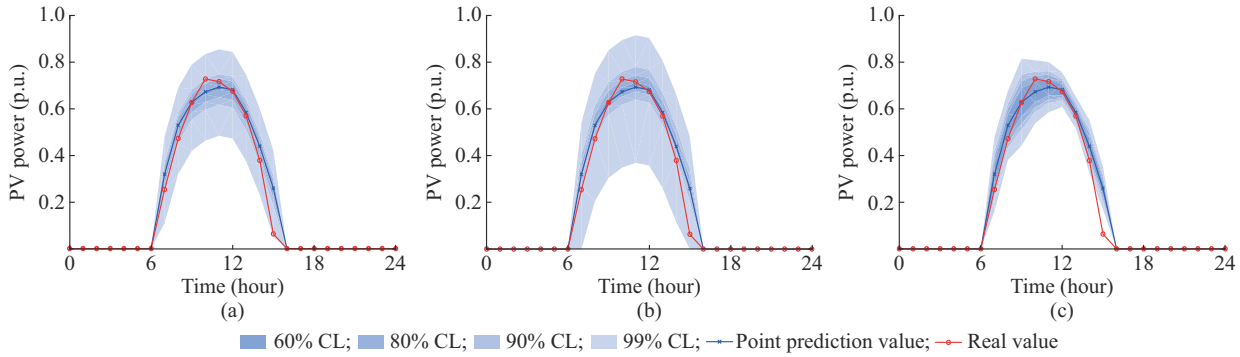

Fig. 14. Prediction errors and real values of PV power at different CLs when using modified bootstrap technique, traditional bootstrap technique, and. ensemble Gaussian model. (a) Modified bootstrap technique. (b) Traditional bootstrap technique. (c) Ensemble Gaussian model.

2) Comparison analysis between modified bootstrap technique and traditional bootstrap technique

Normally, the real values are expected to lie within the lower and upper boundaries of PIs with a prescribed probability (i.e., CL). Comparing the modified bootstrap technique and traditional bootstrap technique in Table I, it is found that the difference between them mainly lies in the size of PICP and CL. The PICP of the modified bootstrap technique is greater than the CL, indicating that the prediction error estimated by the modified bootstrap technique meets the expectation.

Relatively, the PICP of the traditional bootstrap technique is smaller than the CL, showing that the prediction errors estimated by the traditional bootstrap technique fail to cover real values with the prescribed probability. The reason is that the traditional bootstrap technique uses the prediction errors of the training and validation sets to estimate the prediction errors of the test set. In fact, the average prediction error of the training set is smaller than that of the test set, resulting in the PIs constructed by the traditional bootstrap technique is not wide enough to cover real values. This is why the modified bootstrap technique only employs the prediction errors of the validation set to estimate the prediction errors of the test set.

3) Time efficiency of each method

Normally, the real-time system requires an appropriate scheduling scheme within 60 s [34]. During this time, the distribution network acquires observations from sensors and calculates the optimal combination of different power devices. Regarding the time efficiency, the computation time of the modified bootstrap technique, traditional bootstrap technique, and ensemble Gaussian model is 1.13 s, 2.35 s, and 1.28 s, respectively, which indicates their potential to be applied to real-time scheduling of distribution networks.

C. Comparative Analysis of Voltages Between DRPS Model and RRPS Model

The difference in voltages between the DRPS model and RRPS model is clarified in this subsection by discussing the worst-case scenarios (i.e., cases 1 and 2 in Section II).

1) Case 1: voltages cross the lower bound considering uncertainties of power loads of renewable energy sources

First, a sample with a large prediction error is selected. Then, the DRPS and RRPS models are used to obtain the reactive power output schemes of power devices in case 1, as shown in Table II. Finally, the power flow analysis is performed to obtain the voltages of each bus, as shown in Fig. 15.

TABLE II
REACTIVE POWER OUTPUT SCHEMES OF POWER DEVICES IN CASE 1

Model	Tap ratio (%)	Reactive power output (kvar)				
		CB_1	CB_2	WT_1	WT_2	PV_1
DRPS	4×1.25	500	200	299.17	295.69	113.83
RRPS	4×1.25	500	500	299.52	294.37	230.58

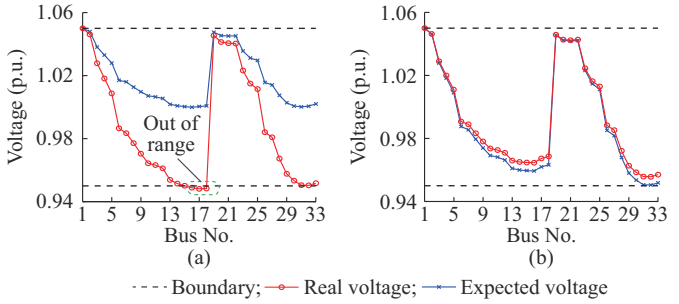

Fig. 15. Voltage of each bus in case 1. (a) DRPS. (b) RRPS.

The objective function of the DRPS model is to minimize the operational cost given point prediction values of power loads and renewable energy sources without considering prediction errors. Under ideal conditions (i. e., point prediction is completely accurate and error free), if the DRPS model-based scheduling scheme is applied to distribution networks, the voltage of each bus is within the safe range, as shown by the blue line in Fig. 15(a). However, the prediction errors of power loads and renewable energy sources are inevitable

in practical engineering. For this specific sample, the real power loads are larger than the point prediction values, while the real active power outputs of the renewable energy sources are smaller than the point prediction values. Therefore, the DRPS model-based scheduling scheme provides insufficient reactive power outputs to support the voltages, and the voltage magnitudes of buses (e.g., the 16th bus to 18th bus) fall below the lower boundary.

In contrast, the RRPS model takes into account the prediction errors of power loads and renewable energy sources by combining point prediction values and prediction errors, and then provides sufficient reactive power to ensure that the voltage is in a safe range for both the worst-case scenario (i.e., the blue line in Fig. 15(b)) and real scenario (i.e., the red line in Fig. 15(b)).

2) Case 2: voltages cross the upper bound considering uncertainties of power loads of renewable energy sources

There may be opposite scenarios to case 1. Specifically, in this case, another sample with a large prediction error is selected. Then, the DRPS and RRPS models are used to obtain the scheduling schemes of power devices in case 2, as shown in Table III. Finally, the power flow analysis is performed to obtain the voltages of each bus, as shown in Fig. 16.

TABLE III
REACTIVE POWER OUTPUT SCHEMES OF POWER DEVICES IN CASE 2

Model	Tap ratio (%)	Reactive power output (kvar)				
		CB_1	CB_2	WT_1	WT_2	PV_1
DRPS	4×1.25	500	100	89.46	124.66	97.95
RRPS	4×1.25	500	200	20.74	17.37	−160.79

Similarly, the DRPS model based scheduling scheme attempts to ensure the security of distribution networks for the deterministic point prediction scenario, as shown by the blue line in Fig. 16(a). Nevertheless, for this specific sample, the real power loads are smaller than the point prediction values, and the real active power outputs of the renewable energy sources are larger than the point prediction values. The difference between the point prediction values and real values causes voltage magnitudes of buses to cross the upper boundary, as shown by the red line in Fig. 16(a).

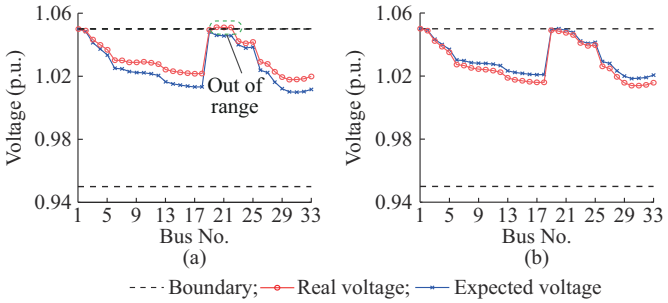

Fig. 16. Voltage of each bus in case 2. (a) DRPS. (b) RRPS.

Relatively, the RRPS model reduces the leading reactive power output and ensures the safety of the distribution network for the possible worst-case scenario and real scenario.

D. Comparative Analysis of Reactive Power Outputs Between DRPS Model and RRPS Model

The difference in reactive power outputs between the DRPS model and RRPS model is clarified in this subsection.

Specifically, a sample is randomly selected. A gated recurrent unit model (i.e., point prediction model) is employed to predict the day-ahead power loads, wind power, and PV power, which are used to obtain a DRPS model based scheduling scheme. To obtain an RRPS model based scheduling scheme, the modified bootstrap techniques are utilized to construct two worst-case scenarios (90% CL is used as a simple example). Finally, Figs. 17 and 18 show the reactive power output schemes of the DRPS model and RRPS model, respectively. Besides, Table IV presents the operational costs and voltage ranges of the DRPS model and RRPS model for one day.

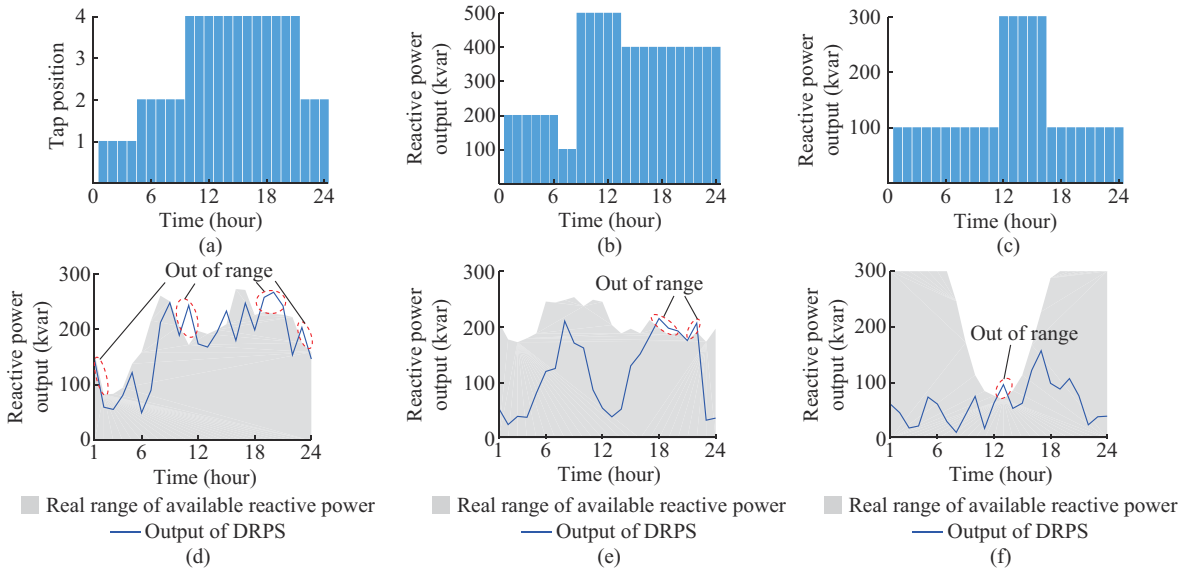

Fig. 17. Reactive power output scheme of DRPS model. (a) Tap position when action times are 3. (b) Reactive power output of CB_1 when action times are 3. (c) Reactive power output of CB_2 when action times are 2. (d) Reactive power output of WT_1. (e) Reactive power output of WT_2. (f) Reactive power output of PV_1.

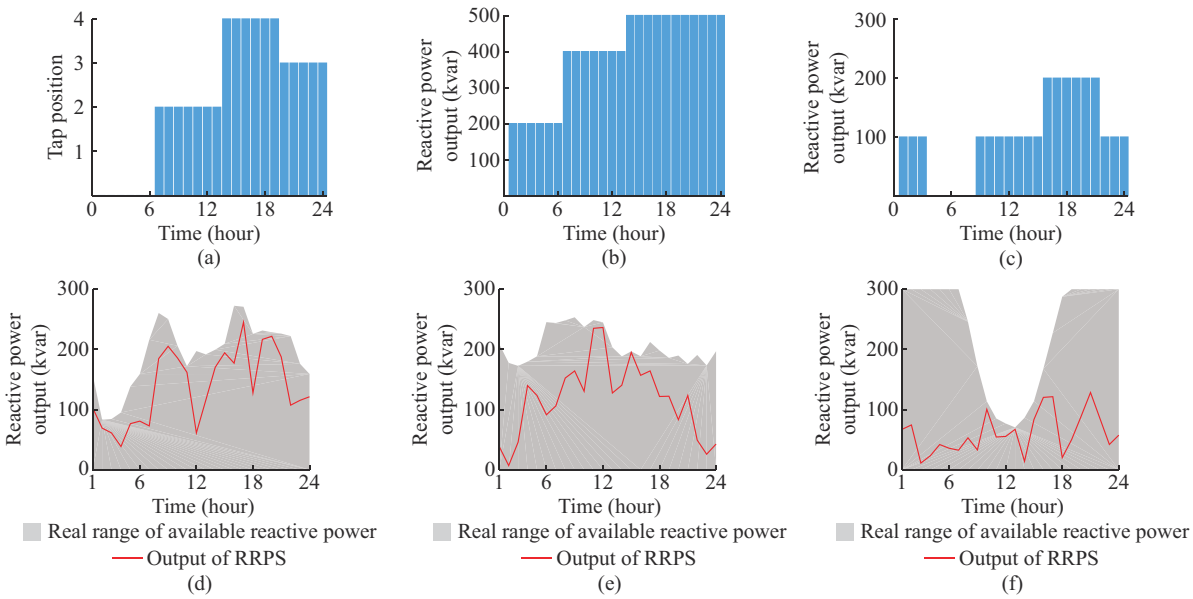

Fig. 18. Reactive power output scheme of RRPS model. (a) Tap position when action times are 3. (b) Reactive power output of CB_1 when action times are 2. (c) Reactive power output of CB_2 when action times are 4. (d) Reactive power output of WT_1. (e) Reactive power output of WT_2. (f) Reactive power output of PV_1.

For the DRPS model-based scheduling scheme, the reactive power outputs of renewable energy sources exceed the real maximum available range at times, making the scheduling scheme unworkable. For example, the planned reactive power output of WT_1 from the 7^{th} hour to the 21^{st} hour is greater than the maximum available reactive power. In contrast, the RRPS model-based scheduling scheme ensures that the outputs of renewable energy sources are always within the maximum available range, as shown in Fig. 17(d) to Fig. 17(f). The reason is that the RRPS model takes into account the uncertainty of the reactive power output through (17).

No matter the DRPS model-based scheduling scheme or the RRPS model-based scheduling scheme, their transformer tap and CBs do not exceed the maximum allowable action times (the maximum allowable action times over 24 hours are 5 for CBs, and the maximum allowable action times over 24 hours are 4 for transformer taps). For example, for the RRPS model-based scheduling scheme, the transformer tap switches 3 times a day, the CB_1 switches 2 times a day, and the CB_2 switches 3 times a day.

After performing the DRPS model-based scheduling scheme, the voltage magnitude crosses the boundary, as shown in column 3 of Table IV. This indicates that the DRPS model cannot guarantee the security of distribution networks. Although the RRPS model can guarantee the security of distribution networks, it pays a higher operational cost as a price, which is the main limitation of robust programming.

TABLE IV
OPERATIONAL COSTS AND VOLTAGE RANGES OF DRPS AND RRPS MODELS FOR ONE DAY

Model	Operational cost (¥)	Voltage range (p.u.)
DRPS	472.37	[0.998, 1.056]
RRPS	487.50	[0.986, 1.050]

E. Comparative Analysis of Economy and Safety

Section IV-C and Section IV-D employ a specific sample to demonstrate the difference between the DRPS model and the RRPS model in terms of voltage and reactive power output. The difference may exist by chance, as it is too dependent on this specific sample. To fully evaluate the performance of the proposed modified bootstrap technique, this subsection analyzes the economy and safety of the DRPS model and RRPS model through all samples in the test set.

For the DRPS model, a gated recurrent unit model is used to predict day-ahead power loads, wind power, and PV power for each sample test set. Then, the DRPS model based on the point prediction values is solved.

For the RRPS model, the traditional method in [8], ensemble Gaussian model, and traditional bootstrap technique are considered as baselines to construct worst-case scenarios. Specifically, the traditional method in [8] does not require point prediction values. It simply divides the worst-case scenarios into two categories: ① the maximum power loads and the minimum output power of renewable energy sources; ② the minimum power loads and the maximum output power of renewable energy sources. In contrast, the ensemble Gaussian model, traditional bootstrap technique, and modified bootstrap technique need point prediction values to estimate prediction errors. Then, worst-case scenarios are constructed by combining point prediction values and prediction errors at different CLs, as represented in (9)-(12).

After the worst-case scenarios are constructed, the RRPS models based on the traditional method in [8], ensemble Gaussian model, traditional bootstrap technique, and modified bootstrap technique (denoted as models A, B, C, and D in Table V) are solved. Table V shows the average operational costs of the test set and the average percentage of insecure scenarios of each model.

TABLE V
AVERAGE OPERATIONAL COSTS OF TEST SET AND AVERAGE PERCENTAGE OF INSECURE SCENARIOS OF EACH MODEL

Model	CL (%)	Average percentage of insecure scenarios (%)	Average operational cost (¥)
DRPS	None	12.86	465.49
Model A	None	0	525.51
Model B	90	8.21	477.15
Model C		3.75	490.14
Model D		1.67	494.31
Model B	99	4.98	483.10
Model C		0.14	503.56
Model D		0	506.98

1) Comparison Analysis of Security

The DRPS model-based scheduling scheme can only ensure the security of the distribution network for most scenarios, while the physical constraints are not satisfied for scenarios with large prediction errors (the percentage of insecure scenarios is 12.86%). The reason is that the DRPS model does not take into account the prediction errors of power loads, wind power, and PV power.

Although the RRPS models based on the ensemble Gaussian model and traditional bootstrap technique reduce the proportion of insecure scenarios to some extent, they cannot always guarantee the security of the distribution network. The reason is that the PIs constructed by the ensemble Gaussian model and traditional bootstrap technique have small PICPs, which have been elaborated in Section IV-B. The RRPS model based on the modified bootstrap technique has a larger PICP than that of the other models (e.g., models based on ensemble Gaussian model and traditional bootstrap technique) at different CLs, which leads to a very small percentage of insecure scenarios. For example, when the CL is 99%, the proportion of insecure scenarios is 0%. This shows that the RRPS model based on the modified bootstrap technique can ensure that the distribution network is always within the physical constraints. Especially, for distribution networks with important loads (e. g., hospitals, transportation hubs, coal mines, chemical plants), power operators expect to find robust solutions where the average percentage of insecure situations is close to 0%. In this case, the RRPS model based on the modified bootstrap technique is a better choice than the RRPS models based on the ensemble Gaussian model and traditional bootstrap technique.

2) Comparison Analysis of Economy

Although the operational costs of the RRPS models based on the ensemble Gaussian model and traditional bootstrap technique are slightly lower than those of the RRPS model based on the modified bootstrap technique, they cannot ensure the security of the distribution network, even if the CL is 99%. Conversely, the percentage of insecure scenarios is 0% for the RRPS model based on the traditional method in [8], but it has the highest operational cost due to over-conservatism.

Further, the RRPS model based on the modified bootstrap technique can be considered a compromise approach that balances economy and security well. For example, when the CL is 99%, the average operational cost of this model is only 8.91% higher than that of the DRPS model, but it reduces the percentage of insecure scenarios by 12.86%. In other words, the RRPS model based on the modified bootstrap technique has higher safety than the DRPS model, the RRPS model based on the ensemble Gaussian model, and the RRPS model based on the traditional bootstrap technique, while it has a better economy than the RRPS model based one the traditional method in [8].

V. CONCLUSION

To solve the risk brought by the uncertainties of power loads and renewable energy sources to distribution networks, this paper proposes a new RRPS model of distribution networks based on a modified bootstrap technique. Simulation and analysis in IEEE 33-bus distribution network lead to the following conclusions.

1) The modified bootstrap technique can accurately capture the uncertainty in power loads, wind power, and PV power. At the same CL, the PICP of PIs generated by the modified bootstrap technique is much larger than that of the traditional ensemble Gaussian model and traditional bootstrap technique, which shows that the worst-case scenarios constructed by the modified bootstrap technique are better than other models to represent all possible scenarios.

2) The traditional DRPS model does not consider the uncertainties of power loads, wind power, and PV power, resulting in the voltages may cross the boundary, especially for extreme scenarios (e. g., case 1 and case 2 discussed in Section IV-C). In contrast, the RRPS model keeps the voltages of the distribution network within a safe range at all time, even in the worst-case scenarios.

3) No matter the DRPS model-based scheduling scheme or the RRPS model-based scheduling scheme is, its transformer taps and CBs do not exceed the maximum allowable action times. For the DRPS model-based scheduling scheme, the outputs of renewable energy sources exceed the real maximum available range at times, making the scheduling scheme unworkable. In contrast, the RRPS model-based scheduling scheme ensures that the outputs of renewable energy sources are always within the maximum available range.

4) The RRPS model based on the modified bootstrap technique balances the economy and security well. It has higher safety than the DRPS model, RRPS model based on the ensemble Gaussian model, and RRPS model based on the traditional bootstrap technique, while it has a better economy than the RRPS model based on the traditional method in [8].

The main limitation of the modified bootstrap technique proposed in this paper is that the operational cost is higher than that of some existing methods, so one of the extensions is to reduce the operational cost.

In addition to centralized scheduling, the RRPS model may be generalized to the distributed optimization scheduling of distribution networks in future works [35]. Theoretically, the modified bootstrap technique-based prediction error estimation and new worst-case scenario construction should be applicable to other robust programming models

(regardless of whether a model is centralized or distributed optimization), since they are independent of the specific optimization model that is actually used.

REFERENCES

[1] Q. Hui, Y. Teng, H. Zuo *et al*., "Reactive power multi-objective optimization for multi-terminal AC/DC interconnected power systems under wind power fluctuation," *CSEE Journal of Power and Energy Systems*, vol. 6, no. 3, pp. 630-637, Sept. 2020.

[2] W. Liao, L. Ge, B. Bak-Jensen *et al*., "Scenario prediction for power loads using a pixel convolutional neural network and an optimization strategy," *Energy Reports*, vol. 8, pp. 6659-6671, Nov. 2022.

[3] Q. Zhao, W. Liao, S. Wang *et al*., "Robust voltage control considering uncertainties of renewable energies and loads via improved generative adversarial network," *Journal of Modern Power Systems and Clean Energy*, vol. 8, no. 6, pp. 1104-1114, Nov. 2020.

[4] S. M. Said, A. Ali, and B. Hartmann, "Tie-line power flow control method for grid-connected microgrids with SMES based on optimization and fuzzy logic," *Journal of Modern Power Systems and Clean Energy*, vol. 8, no. 5, pp. 941-950, Sept. 2020.

[5] N. H. Khan, Y. Wang, D. Tian *et al*., "Fractional PSOGSA algorithm approach to solve optimal reactive power dispatch problems with uncertainty of renewable energy resources," *IEEE Access*, vol. 8, pp. 215399-215413, Nov. 2020.

[6] C. Zhang, H. Chen, K. Shi *et al*., "A multi-time reactive power optimization under interval uncertainty of renewable power generation by an interval sequential quadratic programming method," *IEEE Transactions on Sustainable Energy*, vol. 10, no. 3, pp. 1086-1097, Jul. 2019.

[7] Z. Huang, Y. Zhang, and S. Xie, "Data-adaptive robust coordinated optimization of dynamic active and reactive power flow in active distribution networks," *Renewable Energy*, vol. 188, pp. 164-183, Apr. 2022.

[8] M. A. Mahmud, M. J. Hossain, and H. R. Pota, "Voltage variation on distribution networks with distributed generation: worst case scenario," *IEEE Systems Journal*, vol. 8, no. 4, pp. 1096-1103, Dec. 2014.

[9] Y. Wang, W. Wu, B. Zhang *et al*., "Robust voltage control model for active distribution network considering PVs and loads uncertainties," in *Proceedings of IEEE PES General Meeting*, Denver, USA, Jul. 2015, pp. 1-5.

[10] M. Sun, C. Feng, E. K. Chartan *et al*., "A two-step short-term probabilistic wind forecasting methodology based on predictive distribution optimization," *Applied Energy*, vol. 238, pp. 1497-1505, Mar. 2019.

[11] H. Bidaoui, I. E. Abbassi, A. E. Bouardi *et al*., "Wind speed data analysis using Weibull and Rayleigh distribution functions, case study: five cities northern Morocco," *Procedia Manufacturing*, vol. 32, pp. 786-793, Oct. 2019.

[12] K. A. Singh, M. G. M. Khan, and M. R. Ahmed, "Wind energy resource assessment for cook islands with accurate estimation of Weibull parameters using frequentist and Bayesian methods," *IEEE Access*, vol. 10, pp. 25935-25953, Mar. 2022.

[13] A. S. AI-Sumaiti, M. H. Ahmed, S. Rivera *et al.*, "Stochastic PV model for power system planning applications," *IET Renewable Power Generation*, vol. 13, no. 16, pp. 3168-3179, Dec. 2019.

[14] S. Xu, W. Wu, Y. Yang *et al*., "Analytical solution of stochastic real-time dispatch incorporating wind power uncertainty characterized by Cauchy distribution," *IET Renewable Power Generation*, vol. 15, no. 10, pp. 2286-2301, Jun. 2021.

[15] J. Wu, B. Zhang, H. Li *et al*., "Statistical distribution for wind power forecast error and its application to determine optimal size of energy storage system," *International Journal of Electrical Power & Energy Systems*, vol. 55, pp. 100-107, Feb. 2014.

[16] P. Chen, T. Su, and P. M. Fan, "Thermoelectric energy harvesting interface circuit with capacitive bootstrapping technique for energy-efficient IoT devices," *IEEE Internet of Things Journal*, vol. 5, no. 5, pp. 4058-4065, Oct. 2018.

[17] Y. Maddahi and K. Zareinia, "Nonparametric bootstrap technique to improve positional accuracy in mobile robots with differential drive mechanism," *IEEE Access*, vol. 8, pp. 158502-158511, Sept. 2020.

[18] T. Ding, Q. Yang, Y. Yang *et al*., "A data-driven stochastic reactive power optimization considering uncertainties in active distribution networks and decomposition method," *IEEE Transactions on Smart Grid*, vol. 9, no. 5, pp. 4994-5004, Sept. 2018.

[19] P. Li, Z. Wu, C. Zhang *et al*., "Multi-timescale affinely adjustable robust reactive power dispatch of distribution networks integrated with high penetration of PV," *Journal of Modern Power Systems and Clean Energy*, vol. 11, no. 1, pp. 324-334, Jan. 2023.

[20] L. Zhang, W. Tang, J. Liang *et al*., "Coordinated day-ahead reactive power dispatch in distribution network based on real power forecast errors," *IEEE Transactions on Power Systems*, vol. 31, no. 3, pp. 2472-2480, May 2016.

[21] E. Davoodi, E. Babaei, B. Mohammadi-Ivatloo *et al*., "A novel fast semidefinite programming-based approach for optimal reactive power dispatch," *IEEE Transactions on Industrial Informatics*, vol. 16, no. 1, pp. 288-298, Jan. 2020.

[22] A. Samimi, "Probabilistic day-ahead simultaneous active/reactive power management in active distribution systems," *Journal of Modern Power Systems and Clean Energy*, vol. 7, no. 6, pp. 1596-1607, Jan. 2019.

[23] S. Adhikari, F. Li, and H. Li, "*P-Q* and *P-V* control of photovoltaic generators in distribution systems," *IEEE Transactions on Smart Grid*, vol. 6, no. 6, pp. 2929-2941, Nov. 2015.

[24] A. Ginart and B. Sharifipour, "High penetration of electric vehicles could change the residential power system: public DC fast chargers will not be enough," *IEEE Electrification Magazine*, vol. 9, no. 2, pp. 34-42, Jun. 2021.

[25] W. Liao, S. Wang, B. Bak-Jensen *et al*., "Ultra-short-term interval prediction of wind power based on graph neural network and improved bootstrap technique," *Journal of Modern Power Systems and Clean Energy.* doi: 10.35833/MPCE.2022.000632.

[26] M. Baran and F. Wu, "Network reconfiguration in distribution systems for loss reduction and load balancing," *IEEE Transactions on Power Delivery*, vol. 4, no. 2, pp. 1401-1407, Apr. 1989.

[27] L. Chen, Z. Deng, and X. Xu, "Two-stage dynamic reactive power dispatch strategy in distribution network considering the reactive power regulation of distributed generations," *IEEE Transactions on Power Systems*, vol. 34, no. 2, pp. 1021-1032, Mar. 2019.

[28] UK Power Networks. (2015, Jun.). Low carbon London project. [Online]. Available: https://data. london. gov. uk/dataset/smartmeter-energy-use-data-in-london-households

[29] National Renewable Energy Laboratory. (2012, Nov.). Solar integration national dataset toolkit. [Online]. Available: https://www.nrel.gov/grid/sind-toolkit.html

[30] C. Draxl, A. Clifton, B. Hodge *et al*., "The wind integration national dataset (WIND) toolkit," *Applied Energy*, vol. 151, pp. 355-366, Aug. 2015.

[31] W. Liao, J. Chen, Q. Liu *et al*., "Data-driven reactive power optimization for distribution networks using capsule networks," *Journal of Modern Power Systems and Clean Energy*, vol. 10, no. 5, pp. 1274-1287, Sept. 2022.

[32] W. Liao, B. Bak-Jensen, J. R. Pillai *et al*., "A review of graph neural networks and their applications in power systems," *Journal of Modern Power Systems and Clean Energy*, vol. 10, no. 2, pp. 345-360, Mar. 2022.

[33] C. Sheng, H. Wand, X. Lu *et al*., "Distributed Gaussian granular neural networks ensemble for prediction intervals construction," *Complexity*, vol. 2019, pp. 1-17, Jul. 2019.

[34] Q. Nan. (2016, Jun.). Voltage control in the future power transmission systems. [Online]. Available: https://vbn. aau. dk/ws/portalfiles/portal/254173904/

[35] Z. Yang, W. Liao, Q. Zhang *et al*., "Fault coordination control for converter-interfaced sources compatible with distance protection during asymmetrical faults," *IEEE Transactions on Industrial Electronics*, vol. 70, no. 7, pp. 6941-6952, Jul. 2023.

Wenlong Liao received the B.S. degree from China Agricultural University, Beijing, China, in 2017, and the M.S. degree from Tianjin University, Tianjin, China, in 2020. He is currently pursuing the Ph.D. degree in Aalborg University, Aalborg, Denmark. His current research interests include smart grids, machine learning, and renewable energy.

Shouxiang Wang received the B.S. and M.S. degrees in electrical engineering from Shandong University of Technology, Jinan, China, in 1995 and 1998, respectively, and the Ph.D. degree in electrical engineering from Tianjin University, Tianjin, China, in 2001. He is currently a Professor with the School of Electrical and Information Engineering, and Deputy Director of Key Laboratory of Smart Grid of Ministry of Education, Tianjin University. His main research interests include distributed generation and smart distribution system.

Birgitte Bak-Jensen received the M. Sc. degree in electrical engineering

and the Ph.D. degree in modeling of high voltage components from the Institute of Energy Technology, Aalborg University, Aalborg, Denmark, in 1986 and 1992, respectively. She is currently a Professor with the Department of Energy, Aalborg University. Her current research interests include distribution system analysis, smart grid, and intelligent energy systems.

Jayakrishnan Radhakrishna Pillai received the M.Tech. degree in power systems from the National Institute of Technology, Calicut, India, in 2005, the M.Sc. degree in sustainable energy systems from the University of Edinburgh, Edinburgh, UK, in 2007, and the Ph.D. degree in power systems from Aalborg University, Aalborg, Denmark, in 2011. He is currently an Associate Professor with the Department of Energy, Aalborg University. His current research interests include distribution system analysis, grid integration of electric vehicles and distributed energy resources, smart grids, and intelligent energy systems.

Zhe Yang received the B.S. degree from Northeast Electric Power University, Jilin, China, in 2017, and the M.S. degree from North China Electric Power University, Beijing, China, in 2020. He is currently pursuing the Ph.D. degree in Aalborg University, Aalborg, Denmark. His current research interests include machine learning, renewable energy, and power system protection.